Catalysis Today 174 (2011) 148–159

Contents lists available at ScienceDirect

Catalysis Today

journal homepage: www.elsevier.com/locate/cattod

Synthesis, photocatalytic activities and degradation mechanism of Bi_2WO_6 toward crystal violet dye

Yi-Hsien Ben Liao [a], Jian Xun Wang [a], Jia-Shi Lin [a], Wen-Hsin Chung [b], Wan-Yu Lin [b], Chiing-Chang Chen [a,*]

[a] Department of Science Application and Dissemination, National Taichung University of Education, Taichung 403, Taiwan, ROC
[b] Department of Plant Pathology, National Chung Hsing University, Taichung 402, Taiwan, ROC

ARTICLE INFO

Article history:
Received 26 October 2010
Received in revised form 7 March 2011
Accepted 21 March 2011
Available online 6 May 2011

Keywords:
Bi_2WO_6
Photocatalyst
Hydrothermal autoclave
Photodegradation
Crystal violet

ABSTRACT

Nanocrystalline Bi_2WO_6 (BWO) with square-plates morphology was prepared by the hydrothermal synthesis in autoclave. $Bi(NO_3)_3{\cdot}5H_2O$ with $(NH_4)_{10}W_{12}O_{41}{\cdot}5H_2O$ was reacted in pH 9 solution at 160 °C for 24 h, 48 h and 72 h to yield the resulting Bi_2WO_6 as a white precipitate. Bi_2WO_6 was characterized by the field emission scanning electron microscopy with the energy dispersive X-ray spectrometer (FE-SEM–EDS), the X-ray diffractrommeter (XRD), and the high resolution X-ray photoelectron spectroscopy (HR-XPS). The XPS spectra showed a binding energy shift of Bi element, suggesting that the $Bi^{(+3-x)}$ formal oxidation state could be the substoichiometric forms of Bi within the Bi_2O_2 layer. The photocatalytic activities of the prepared BWO samples were evaluated by the photodegradation of crystal violet (CV) dye under UV-light irradiation (365 nm). The intermediates were separated and characterized by HPLC-PDA-ESI/MS techniques and the results indicate that the *N*-de-methylation with oxidative degradation of the crystal violet dye took place. Based on these intermediates, we propose and discuss the degradation pathways.

1. Introduction

The transition metal oxide-based nanomaterials with wide variety of structures offer promising applications in various field of study. Bi_2WO_6 (BWO) is known as one of a member of the Aurivillius family with layered perovskites, which structurally are comprised of alternating perovskite-like and fluorite-like blocks, with general formula of $[Bi_2O_2][WO_4]$ [1]. The perovskite block consists of an infinite two-dimensional array of corner-linked WO_6 octahedra alternating with $[Bi_2O_2]_n^{2+}$ slabs [2,3]. Recently BWO has attracted considerable research attention for its distinguished physical and chemical properties, e.g. oxide anion conductivity [4], nonlinear dielectric susceptibility [5], and piezoelectrity/ferroelectricity [6]. Furthermore, BWO is a highly promising photocatalyst that is capable of degrading organic compounds [7–13] under visible light irradiation.

These environmentally important properties have aroused general interest in the nanostructures of BWO and its superior photocatalytic properties compared to those of the bulk material [14–17]. Thus considerable research attention has recently been focused on the fabrication of BWO with various nanostructures [18–22], including agglomerated states of BWO in single crystal, in solid solution, in film, in glass, and so on. The literature reported synthetic methods were mostly by the solid-state reaction [23], by flux growth [24], by the sol–gel method [25], by the coprecipitation method [26], and by the hydrothermal method [27–30]. The preparation conditions of the hydrothermal syntheses usually involve organic templates, which exercise considerable influences over the resulting material's properties via different mechanism [31–33]. This indicates that hierarchically structured BWO is not only an outstanding multifunctional material, but also an excellent model system for obtaining new insights into the general relationship among synthesis, morphology, and properties in nanomaterial fabrication.

In early reports [34,35], studies focused on the nanostructure of BWO photocatalysts, the effects of study conditions, and possible environmental application. Few fundamental studies have been conducted on BWO-assisted photocatalytic degradation for organics under visible light irradiation. The mechanistic studies on BWO-assisted photocatalytic degradation for triphenylmethane dye under UV irradiation have never been reported before. Accordingly, this study focuses on the separation and identification of the photocatalytic reaction intermediates in hopes of shedding some light on the mechanistic details of BWO-assisted UV photodegradation of the crystal violet (CV) dye as a foundation for their potential environmental applications.

* Corresponding author. Tel.: +886 4 2218 3406; fax: +886 4 2218 3560.
E-mail address: ccchen@mail.ntcu.edu.tw (C.-C. Chen).

0920-5861/$ – see front matter © 2011 Elsevier B.V. All rights reserved.
doi:10.1016/j.cattod.2011.03.048

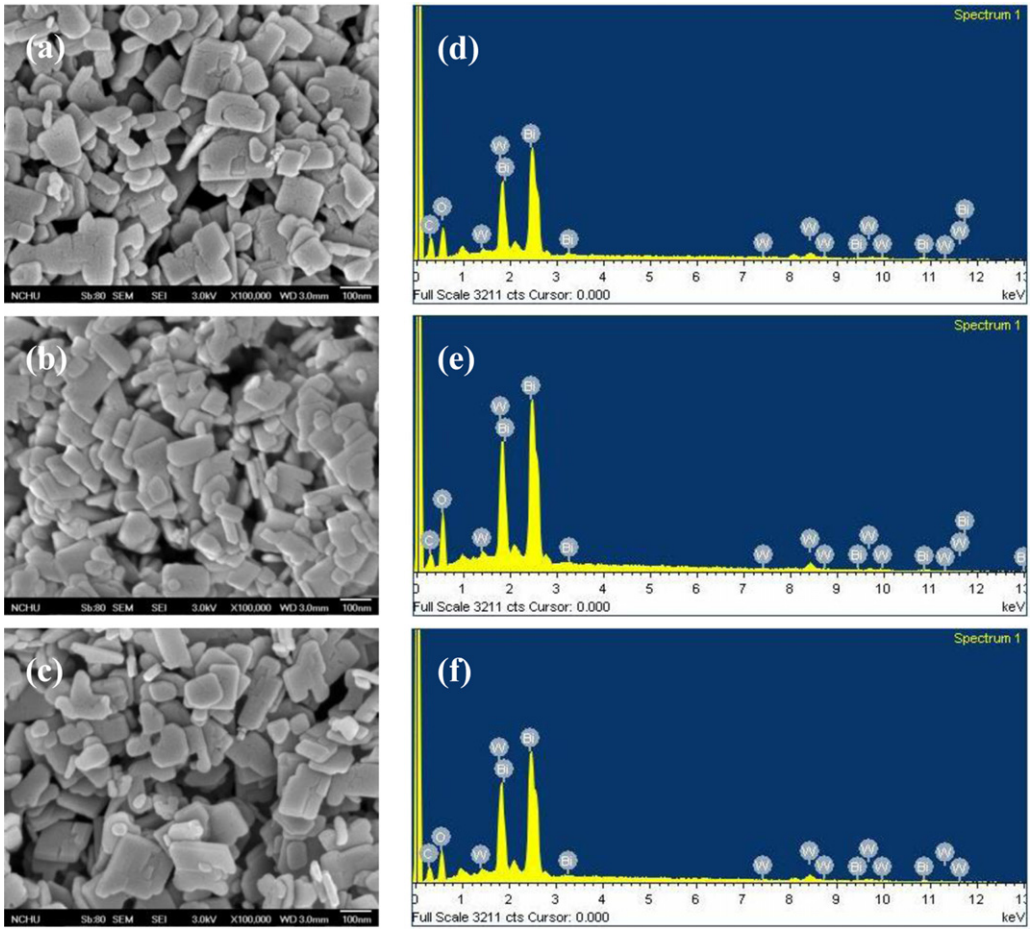

Fig. 1. SEM images and EDS of Bi_2WO_6 with the nanoplates structures prepared by the hydrothermal method at 160 °C; for 24 h (a) (d); for 48 h (b) (e); for 72 h (c) (f).

2. Experimental

2.1. Materials and preparation of photocatalysts

$Bi(NO_3)_3{\cdot}5H_2O$, $(NH_4)_{10}W_{12}O_{41}{\cdot}5H_2O$ (Aldrich) and CV dye (TCI) were obtained and used without any further purification. Reagent-grade ammonium acetate, sodium hydroxide, nitric acid and HPLC-grade methanol were purchased from Merck. The de-ionized water used for this study was purified with a Milli-Q water ion-exchange system (Millipore Co.) for a resistivity of $1.8 \times 10^7\ \Omega$ cm.

4 mmol of $Bi(NO_3)_3{\cdot}5H_2O$ and 0.17 mmol of $(NH_4)_{10}W_{12}O_{41}{\cdot}5H_2O$ were added into a 100 mL flask, followed by the addition of 20 mL of ethyleneglycol. Under stirring, 25% NH_3 was added dropwised to adjust the pH value to 9. A white precipitate was formed and the mixture was transferred into a 30 mL Teflon-lined autoclave. The autoclave was then heated to 160 °C for 24, 48, and 72 h and then cooled to room temperature. After filtration and thoroughly wash with de-ionized water, the resulting white precipitate of the products were characterized by scanning electron microscopy–energy dispersive spectroscopy (SEM–EDS), the powder X-ray difractrommeter (XRD) and a high resolution X-ray photoelectron spectrometer (HR-XPS). The BET specific surface areas of the samples were measured with an automatic system (Micromeritics Gemini 2370C) using nitrogen gas as the adsorbate at liquid nitrogen temperature.

2.2. Instruments

The Waters ZQ LC/MS system, equipped with a binary pump, a photodiode array detector, an autosampler, and a micromass detector, were applied for separation and identification. X-ray powder diffraction (XRD) patterns were recorded on a MAC Science, MXP18 X-ray diffractometer with Cu Kα radiation, operated at 40 kV and 80 mA. Field emission scanning electron microscopy (FESEM) measurement was carried out with a field-emission microscope (JEOL JSM-7401F) at an acceleration voltage of 15 kV. An HR-XPS measurement was carried out with ULVAC-PHI XPS. The Al Kα radiation was generated with a voltage of 15 kV.

Table 1
Physical and chemical properties of the prepared Bi_2WO_6.

Catalyst code	Reaction time (h)	Specific surface area (m^2/g)	Pore volume (cm^3/g)	XPS element atomic (%)				EDS element atomic (atomic %)			
				W	Bi	O	C	W	Bi	O	C
A24	24	25.5850	12.4973	7.78	24.02	50.62	17.48	3.11	6.97	38.95	50.07
A48	48	35.6972	11.9210	11.08	26.35	45.05	17.51	4.39	9.41	57.91	28.29
A72	72	40.5196	12.1664	9.18	26.63	49.09	15.10	4.42	9.45	43.44	42.70

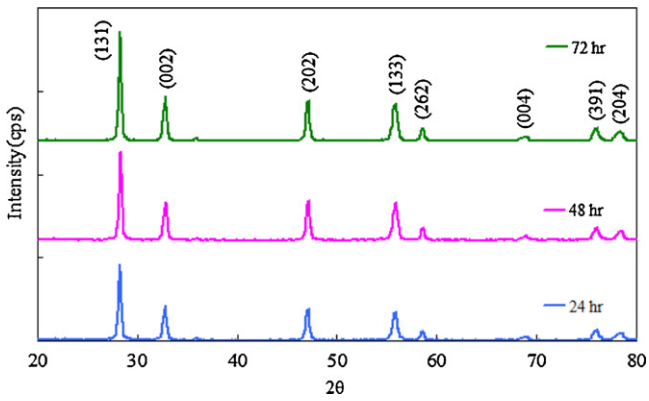

Fig. 2. X-ray diffraction patterns of the Bi_2WO_6 prepared by hydrothermal method at 160 °C for various times.

2.3. Procedure and analysis

Aqueous suspensions of CV (100 mL, 50 ppm) with the given amount of catalyst powder was placed in a Pyrex flask. The pH value of the suspensions was adjusted by either NaOH or HNO_3 solutions. Prior to irradiation, the suspensions were magnetically stirred in the dark for ca. 30 min to establish an adsorption/desorption equilibrium between the dye and the surface of the catalyst under ambient air-equilibrated conditions. Irradiations were carried out using UV-365 nm lamps (20 W). At given irradiation time intervals, 5 mL aliquots were collected and centrifuged to remove the catalyst particulates. The supernatant were analyzed by HPLC-PDA-ESI-MS after readjusting the chromatographic conditions to make the mobile phase compatible with the working conditions of the mass spectrometer.

3. Results and discussion

3.1. Characterization of the synthesized-photocatalysts

Samples of Bi_2WO_6 were prepared by the hydrothermal method in teflone lined autoclave at 160 °C for various length of time. The surface morphology of the prepared photocatalysts was examined by FE-SEM (Fig. 1). The samples exhibited a plate-like rectangular shape with a lateral size of several hundred nanometers and a thickness between 10 and 20 nm. The similar plate-like rectangular-shaped BWO has recently been reported by several research groups [32]. EDS further confirmed the elementary chemical composition of the synthesized products. The physical and chemical properties of the prepared samples are listed in Table 1. The EDS and HR-XPS results showed that the product's main elements are tungsten, bismuth, oxygen, and carbon. The W/Bi atomic ratio of the prepared samples were corresponded well with the expected atomic ratio of BWO (W/Bi = 1/2). The superfluous elemental content of the oxygen and the carbon in the examined product possibly were due to the ethyleneg-

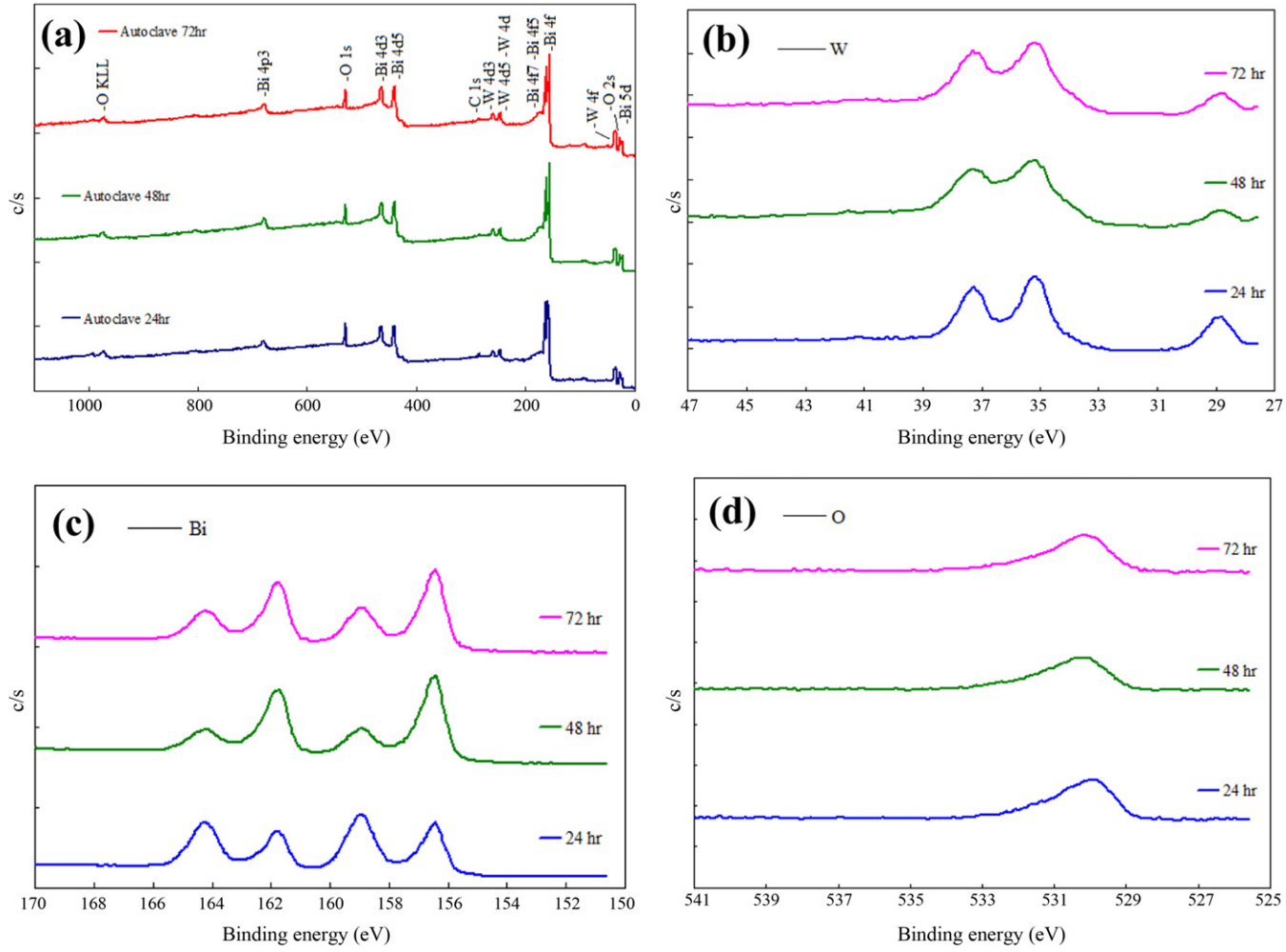

Fig. 3. High resolution XPS spectra of the prepared Bi_2WO_6: (a) Total survey; (b) W 4f; (c) Bi 4f; (d) O 1s.

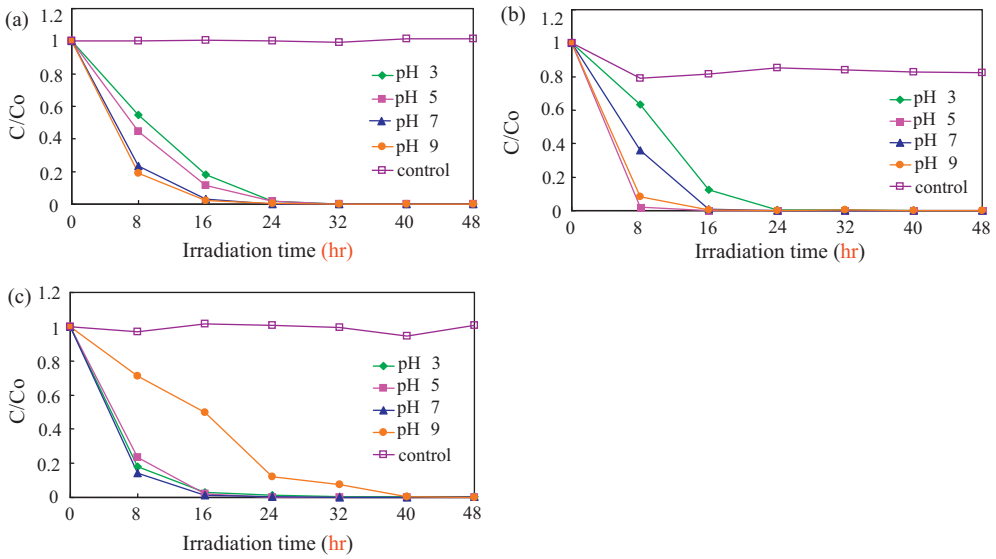

Fig. 4. pH effect on the CV photodegradation rate with concentrations of CV being 0.05 g L^{-1} and Bi_2WO_6 being 0.5 g L^{-1} for (a) A24; (b) A48; (c) A72.

lycol remained under the reaction condition. In addition, the BET results revealed that the specific surface areas of the prepared BWO photocatalysts are 25.6, 35.7 and 40.5 m^2/g for A24, A48, and A72, respectively. These results clearly showed increatment of specific surface area along the progress of hydrothermal reaction time. Similar increatment trend was observed in pore volumes for the prepared BWO photocatalysts as indicated in Table 1.

The crystallinity and phase purity of the products were also examined by the XRD. As the reaction time progressed, the dominant peaks of the XRD patterns were observed at 2θ of 28.3°, 32.7°, 47.1°, 55.8°, 58.5°, 68.7°, 75.9°, and 78.3°, as shown in Fig. 2. These peaks are indexed to the crystalline structure of Russellite Bi_2WO_6 (JCPDS Card No. 79-2381), and respectively correspond to the indices of (1 3 1), (0 0 2), (2 0 2), (1 3 3), (2 6 2), (0 0 4), (3 9 1), and (2 0 4) crystalline planes. Similar features and intensities were found in all samples, indicating that under the reaction condition the hydrothermal reaction can obtain good quality crystal in the range of treating time. No diffraction peaks for the other crystallites were detected.

HR-XPS results for the prepared Bi_2WO_6 samples, including the total survey spectra (Fig. 3(a)), the W 4f spectra (Fig. 3(b)), the Bi 4f spectra (Fig. 3(c)), and the O 1s spectra (Fig. 3(d)) are shown. The binding energy of 37.3 eV and 35.1 eV were referred to the W $4f_{5/2}$ and $4f_{7/2}$, respectively, which can be assigned to the W at the hexavalent oxidation state [36]. The characteristic binding energies of 159.0 eV for Bi $4f_{7/2}$ with side absorption band of 156.4 eV revealed mixed oxidation state of bismuth. It was suggested that the trivalent bismuth was partly reduced to the lower valence state and the ethylene glycol may serve as both the solvent and the reductant during the hydrothermal reaction conditions [30,37] and a similar binding energy shift of 2.3 eV for Bi $4f_{7/2}$ was also observed by Jovalekic et al. [38]. They concluded that the $Bi^{(+3-x)}$ could be attributed to the substoichiometric forms of Bi at the Bi_2O_2 layer and the formation of Bi with low oxidation state resulted the oxygen vacancy in the crystal lattice. As Fig. 3(c) shown, the content of the low valent oxidation state for the bismuth increased as reaction time progressed. Fig. 3(d) showed that the oxygen element may be referred two kinds of chemical states: crystal lattice oxygen and surface adsorbed oxygen [39].

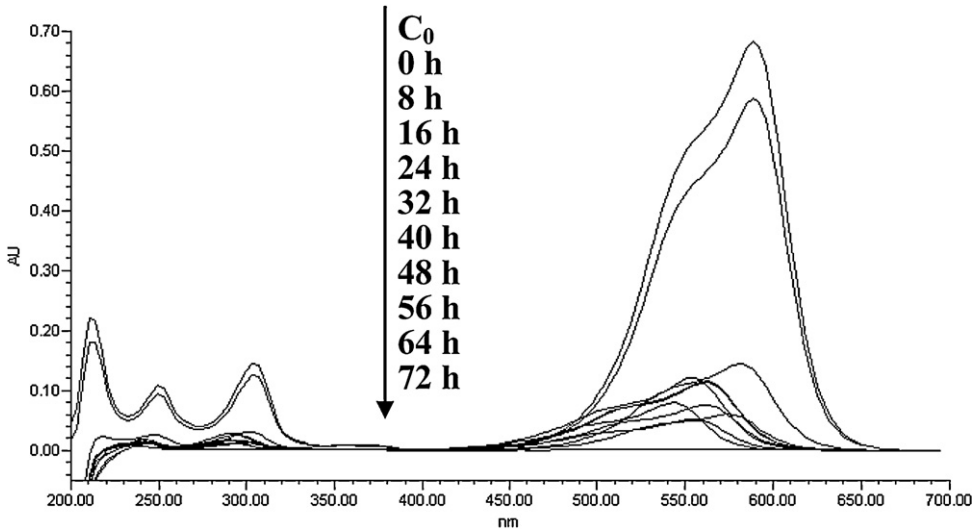

Fig. 5. UV–Vis spectra of degraded CV in aqueous Bi_2WO_6 suspensions.

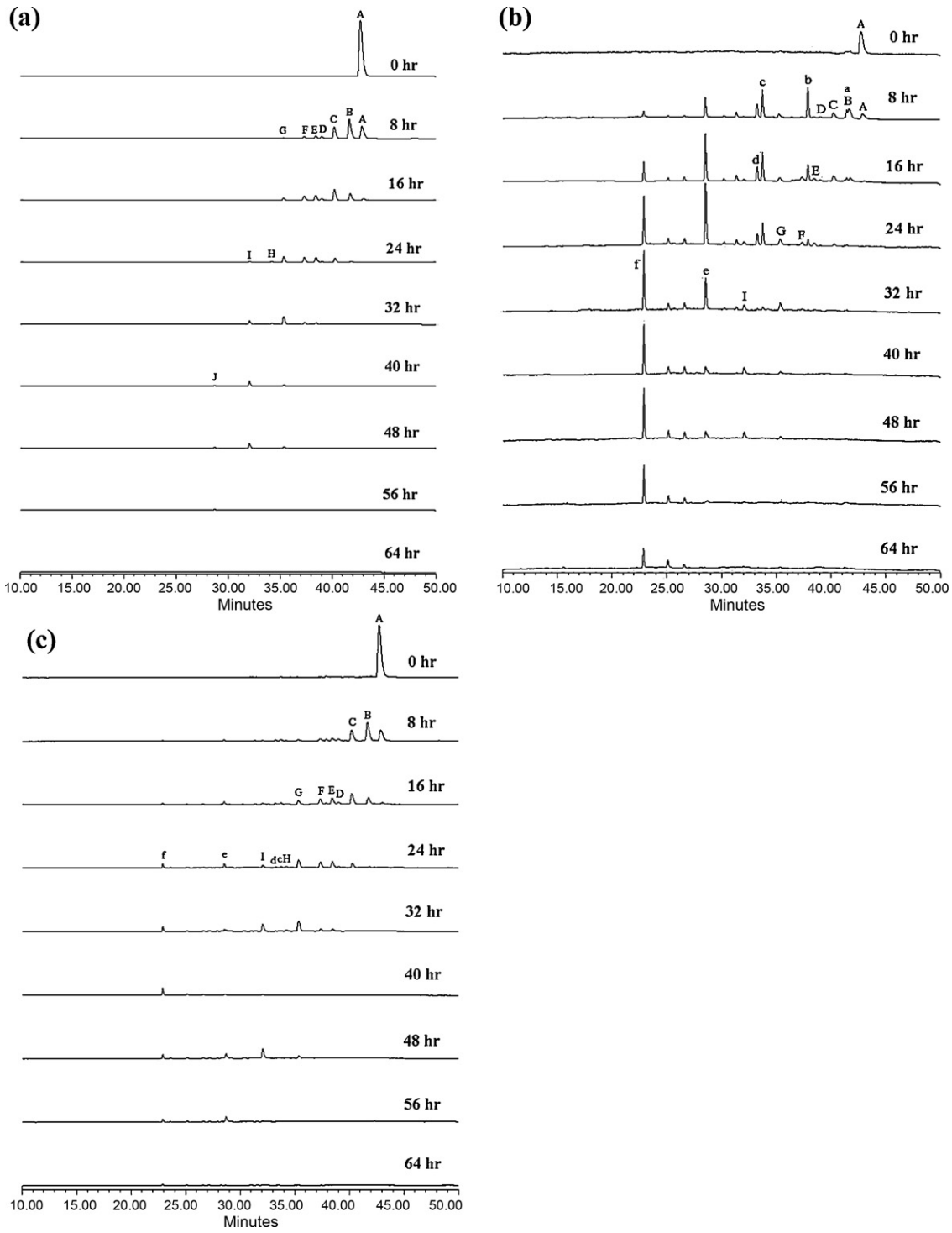

Fig. 6. HPLC/PDA chromatograms of the degradation intermediates at different irradiation intervals, recorded at (a) 580 nm, (b) 350 nm and (c) 300 nm.

3.2. Photocatalytic activity

In photocatalytic processes, the amount of photocatalyst is an important parameter that can affect the degradation rate of organic compounds. Catalyst optimization depends on the nature of the powders [40]. Hence, the effect of photocatalysts on the photodegradation rates of the CV dye was investigated by employing various samples with different length of hydrothermal time (ranging from 24 to 72 h) at various pH conditions (Fig. 4). The photodegradation rate of the CV was found to be optimal when photocatalyst A48 was employed at 0.5 g L^{-1} amount ratio and at pH 9 conditions. The adsorption resulted in a decrease of 1.2%, 20%, and 3.2% in the CV concentration after 8 h at dark condition. Photocatalytic efficiencies were recorded under the UV (365 nm) irradiation which yielded of 80.1%, 98.2%, and 88.4% for the photocatalysts A24, A48 and A72, respectively, at the pH 9. A coherent tendency of physical adsorption and chemical photodegradation behaviors were observed in this study.

Under the conditions of pH above pHzpc (zero point charge), the surface of the photocatalyst easily negatively adsorbs cationic

Table 2
Summary of the CV photocatalytic degradation intermediates identified by the HPLC-PDA-ESI/MS.

HPLC peaks	De-methylation intermediates	Abbreviation	ESI/MS molecular ions (*m*/*z*)	Adsorption maximum (nm)
A	*N*,*N*,*N*′,*N*′,*N*″,*N*″-hexamethyl-pararosaniline	CV	377.2	588.5
B	*N*,*N*-dimethyl-*N*′,*N*′-dimethyl-*N*″-methyl-pararosaniline	DDMPR	358.2	581.2
C	*N*,*N*-dimethyl-*N*′-methyl-*N*″-methyl-pararosaniline	DMMPR	344.2	573.9
D	*N*,*N*-dimethyl-*N*′,*N*′-dimethyl-pararosaniline	DDPR	344.2	577.5
E	*N*-methyl-*N*′-methyl-*N*″-methyl-pararosaniline	MMMPR	330.1	566.5
F	*N*,*N*-dimethyl-*N*′-methyl-pararosaniline	DMPR	330.2	570.2
G	*N*-methyl-*N*′-methyl-pararosaniline	MMPR	316.1	562.9
H	*N*,*N*-dimethyl-pararosaniline	DPR	316.1	566.5
I	*N*-methyl-pararosaniline	MPR	302.1	555.5
J	Pararosaniline	PR	288.1	544.5
a	4-(*N*,*N*-dimethylamino)-4′-(*N*′,*N*′-dimethylamino)benzophenone	DDBP	269.1	376.4
b	4-(*N*,*N*-dimethylamino)-4′-(*N*′-methylamino)benzophenone	DMBP	255.1	366.3
c	4-(*N*-methylamino)-4′-(*N*′-methylamino)benzophenone	MMBP	241.1	362.9
d	4-(*N*,*N*-dimethylamino)-4′-aminobenzophenone	DBP	241.0	362.9
e	4-(*N*-methylamino)-4′-aminobenzophenone	MBP	227.1	357.0
f	4,4′-Bis-aminobenzophenone	BP	213.1	342.6
α	4-(*N*,*N*-dimethylamino)phenol	DAP	N/A	N/A
β	4-(*N*-methylamino)phenol	MAP	N/A	N/A
γ	4-Aminophenol	AP	N/A	N/A

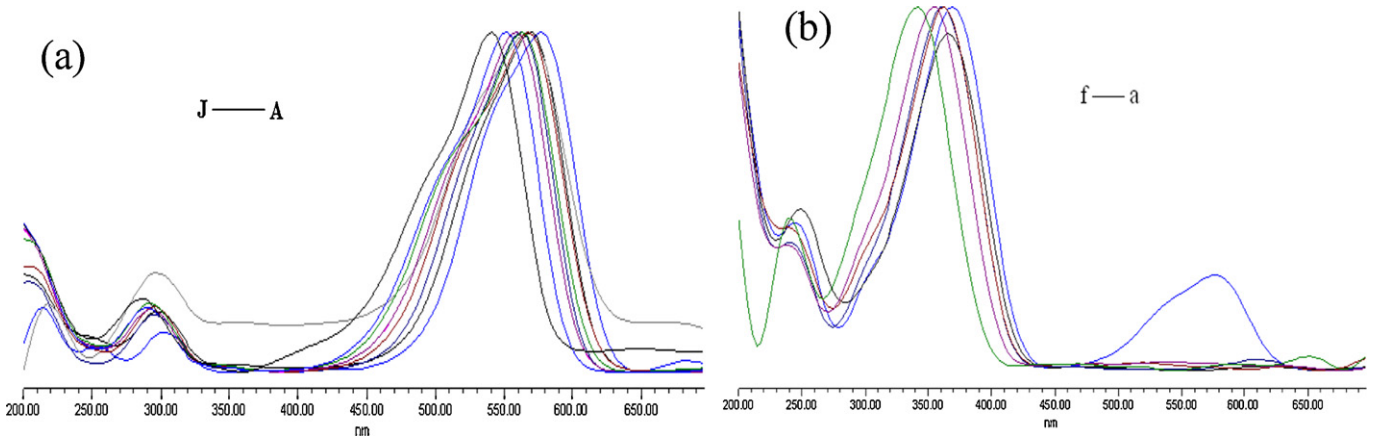

Fig. 7. UV–Vis absorption spectra of the photodegradation intermediates of the CV dye, corresponding to the peaks assigned for (a) **A** to **J** and (b) **a** to **f** in Fig. 6.

species while, under the reverse conditions, anionic species are adsorbed [41]. The adsorption of the substrate onto the Bi_2WO_6 surface directly affects the occurrence of electron transfer between the excited dye and Bi_2WO_6, and further influences the degradation rate. The photodegradation rates of the CV dye at various pH is shown in Fig. 4. The photodegradation rate was found to increase with the solution pH value. The formation of active •OH species is favored at basic conditions, not only due to the improvement of the holes transference to the adsorbed hydroxyls at high pH conditions, but also for the electrostatic abstractive effect between the negatively charged Bi_2WO_6 film and the cationic dyes in the solution. Our results indicate that the Bi_2WO_6 surface was negatively charged, and the CV adsorb onto the Bi_2WO_6 surface through the positive ammonium groups. The proposed adsorption mechanisms are in good agreement with earlier reports [42]. Although the CV dye can, to some extent, adsorb onto the Bi_2WO_6 surface in alkaline media, when the pH value is over 10, the dye molecule will transform into a colorless carbinol base [43].

3.3. UV–Vis spectra

The aqueous solution of the CV dye was fairly stable under UV radiation in the absence of the Bi_2WO_6. However, the CV dye can be degraded rather effectively in aqueous Bi_2WO_6 dispersion under 365 nm UV irradiation. The changes of the UV–Vis spectra during the photodegradation process of the CV dye in the aqueous Bi_2WO_6 dispersions are illustrated in Fig. 5. After UV irradiation for 72 h, ca. 99.8% of the CV dye was degraded. The characteristic absorption band of the CV dye at 588.3 nm decreased rapidly with slight hypsochromic shifts (544.5 nm), without additional absorption bands appeared in the ultraviolet range, indicating that there might be a formation of series of *N*-de-methylated intermediates and cleavages of the whole conjugated chromophore structure of the CV dye. Increasing the irradiation time resulted the decrease of the absorption band at 544.5 nm, but no further wavelength shift was observed, indicating that the absorption band at 544.5 nm is that of the full *N*-de-methylated product of the CV dye.

3.4. Separation of the intermediates

Temporal variations occurring in the solution of CV dye during the degradation process under UV irradiation were examined by HPLC coupled with a photodiode array detector and the ESI mass

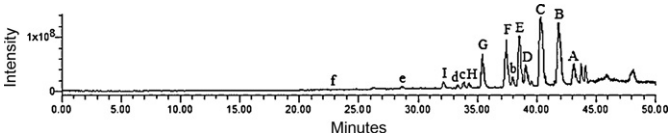

Fig. 8. HPLC/MS chromatogram of the photodegradation intermediates derived from CV.

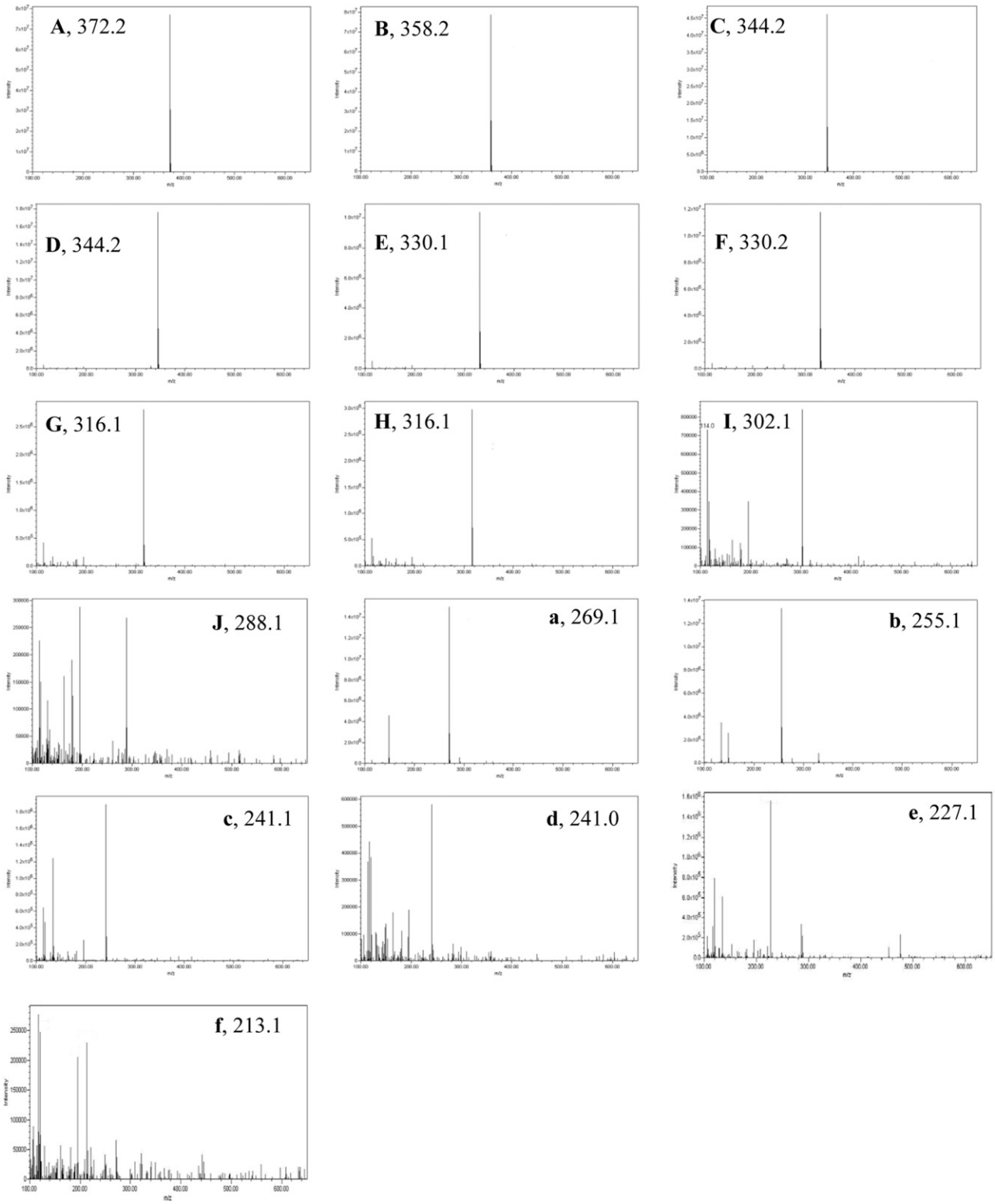

Fig. 9. ESI mass spectra of CV dye photodegradation intermediates **A**–**J**, **a**–**f**.

spectrometry. The HPLC-PDA chromatograms recorded at 580, 350, and 300 nm for the pH 5 solution photodegradation condition are illustrated in Fig. 6. Given irradiation of up to 64 h, 16 intermediates were identified within 50 min retention time. We denoted the CV dye and its related intermediates as species **A**–**J**, and **a**–**f** (Table 2). Except the CV dye (peak **A**), the peaks area of the others initially increased before subsequently decreasing, indicating formation and transformation of the intermediates.

3.5. Identification of the intermediates

3.5.1. UV–Vis spectra of the intermediates

The maximum absorption of each intermediates in the UV–Vis spectral region are depicted in Table 2, corresponding to the assigned peaks **A**–**J** and **a**–**f** in the chromatogram, respectively (Fig. 6). The full scan spectrum for each intermediate is given in Fig. 7. As Fig. 7(a) shown, the maximum absorption

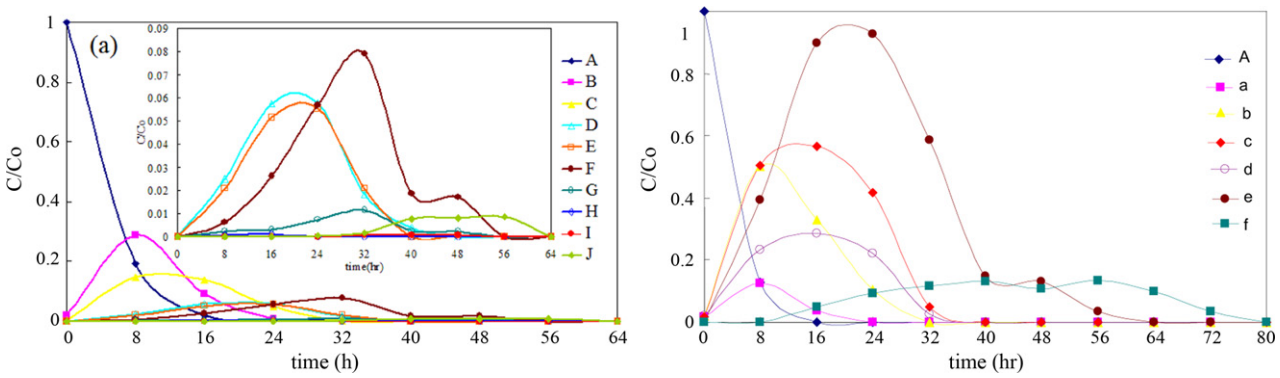

Fig. 10. Variations in the relative distribution of the intermediates obtained from the photodegradation of CV as a function of irradiation time.

bands of intermediates **A**–**J** shifted from 588.5 nm to 544.5 nm. Fig. 7(b) showed the spectra for the intermediates **a**–**f**, which shifted their maximum absorption bands from 376.4 nm to 342.6 nm. These shifts of the absorption bands are presumed to result from the formation of a series of *N*-de-methylated intermediates.

From these results, several groups of intermediates can be distinguished. The first group is marked in the chromatogram and illustrated in Fig. 7(a). The wavelength position of the major absorption band of CV dye *N*-de-methylated intermediate has moved toward the blue region, λ_{max} of **A**, 588.5 nm; **B**, 581.2 nm; **C**, 573.9 nm; **D**, 577.5 nm; **E**, 566.5 nm; **F**, 570.2 nm; **G**, 562.9 nm; **H**, 566.5 nm; **I**, 555.5 nm; **J**, 544.5 nm. The *N*-de-methylation of the CV dye caused the wavelength shifts as depicted in Table 2 due to an attack by one of the active oxygen species on the *N*,*N*-dimethyl or *N*-methyl group. It has previously been reported that the *N*-de-methylation reaction occurred over CV dye is in a stepwise manner (i.e., methyl groups were removed one by one as observed by the gradual band wavelength shifts toward the blue region) [44], and this is confirmed by Table 2.

The second intermediates group was marked in the chromatogram (Fig. 6(b)) and PDA spectra were illustrated in Fig. 7(b). The oxidative destruction of CV yields DAP(α), DDBP(a), and their subsequent intermediates resulted from the following *N*-de-methylation reaction. This is confirmed from the resulting blue shift of the major absorption band with λ_{max}: **a**, 376.4 nm; **b**, 366.3 nm; **c**, 362.9 nm; **d**, 362.9 nm; **e**, 357.0 nm; **f**, 342.6 nm. The proposed intermediate (**a**) has been compared with a standard material of 4-(*N*,*N*-dimethylamino)-4′-(*N*′,*N*′-dimethylamino)benzophenone. The retention time and PDA absorption spectra are identical.

3.5.2. *ESI-mass spectra of the intermediates*

The intermediates were further identified by the HPLC-ESI mass spectrometry, and the relevant mass spectra are illustrated in Figs. 8 and 9 and Table 2. The molecular ion peaks appeared in the protonated forms of the intermediates. The results of mass spectral analysis confirmed that the component **A**, m/z = 372.2, in liquid chromatogram is CV. The other components are: **B**, m/z = 358.2; **C**, m/z = 344.2; **D**, m/z = 344.2; **E**, m/z = 330.1; **F**, m/z = 330.2; **G**, m/z = 316.1; **H**, m/z = 316.1; **I**, m/z = 302.1; **J**, m/z = 288.1; **a**, m/z = 269.1; **b**, m/z = 255.1; **c**, m/z = 241.1; **d**, m/z = 241.0; **e**, m/z = 227.1; **f**, m/z = 213.1.

3.6. *Photodegradation mechanisms of CV*

The relative distribution of the intermediates is illustrated in Fig. 10. To minimize errors, the relative intensities were recorded at the maximum absorption wavelength for each intermediate, although a quantitative determination of all of the photogenerated intermediates was not achieved owing to the lack of appropriate molar extinction coefficients for each of them and to a lack of reference standards. The distributions of all of the *N*-de-methylated intermediates are relative to the initial concentration of CV. Nonetheless, we clearly observed changes in the distribution of each intermediate during the photodegradation of CV. The successive appearance of each intermediate indicated that the *N*-de-methylation of CV and a, is a stepwise photochemical process.

3.6.1. *N-de-methylation of CV*

Most of the •OH radicals are generated either directly from the reaction between the holes and surface-adsorbed H_2O or OH^-. O_2^{-}• would be much less likely to be formed than •OH under UV irradiation [41–44]. The *N*-de-methylation of the CV dye occurred most likely through the attack of the •OH species toward the *N*,*N*-dimethyl group on the CV molecule. The degradation intermediates were clearly observed to reach their maximum concentrations (Fig. 10). The concentration of the other intermediates may be too low to be examined by the HPLC-PDA-ESI/MS. The results discussed above can be seen more clearly in Fig. 11. The CV approached the negatively charged Bi_2WO_6 particle surface via the positive charged dimethylamine group. Before the conjugated aminotriphenylmethane structure was destroyed, the *N*-de-methylation occurred preferentially yielding the major products *N*-de-methylated CV species.

3.6.2. *Oxidative degradation of the CV*

The degradation of the CV dye may also occur through attack of the •OH species on the central carbon of the CV via the conjugated structure of the aminotriphenylmethane and produced intermediates a and α. The degradation intermediates were clearly observed in Fig. 10 to reach their maximum concentrations. The results can be seen more clearly as depicted in Fig. 12. Further evidences for the pathway(s) of photodegradation were reported previously in our study with GC–MS spectrometry [45].

3.6.3. *The pathways of photocatalytic degradation of the CV*

According to the earlier reports [46,47], most *N*-de-alkylation processes were preceded by the formation of a nitrogen-centered radical while destruction of dye chromophore structures is preceded by the generation of a carbon-centered radical. Consistent with this, degradation of CV must occur via two different photodegradation pathways (destruction of the chromophore structure and *N*-de-methylation) due to the formation of different radicals (either a carbon-centered or nitrogen-centered radical). There is no doubt that the •OH attack on the dye yielded a cationic radical dye•$^+$, which can then undergo hydrolysis and/or follow var-

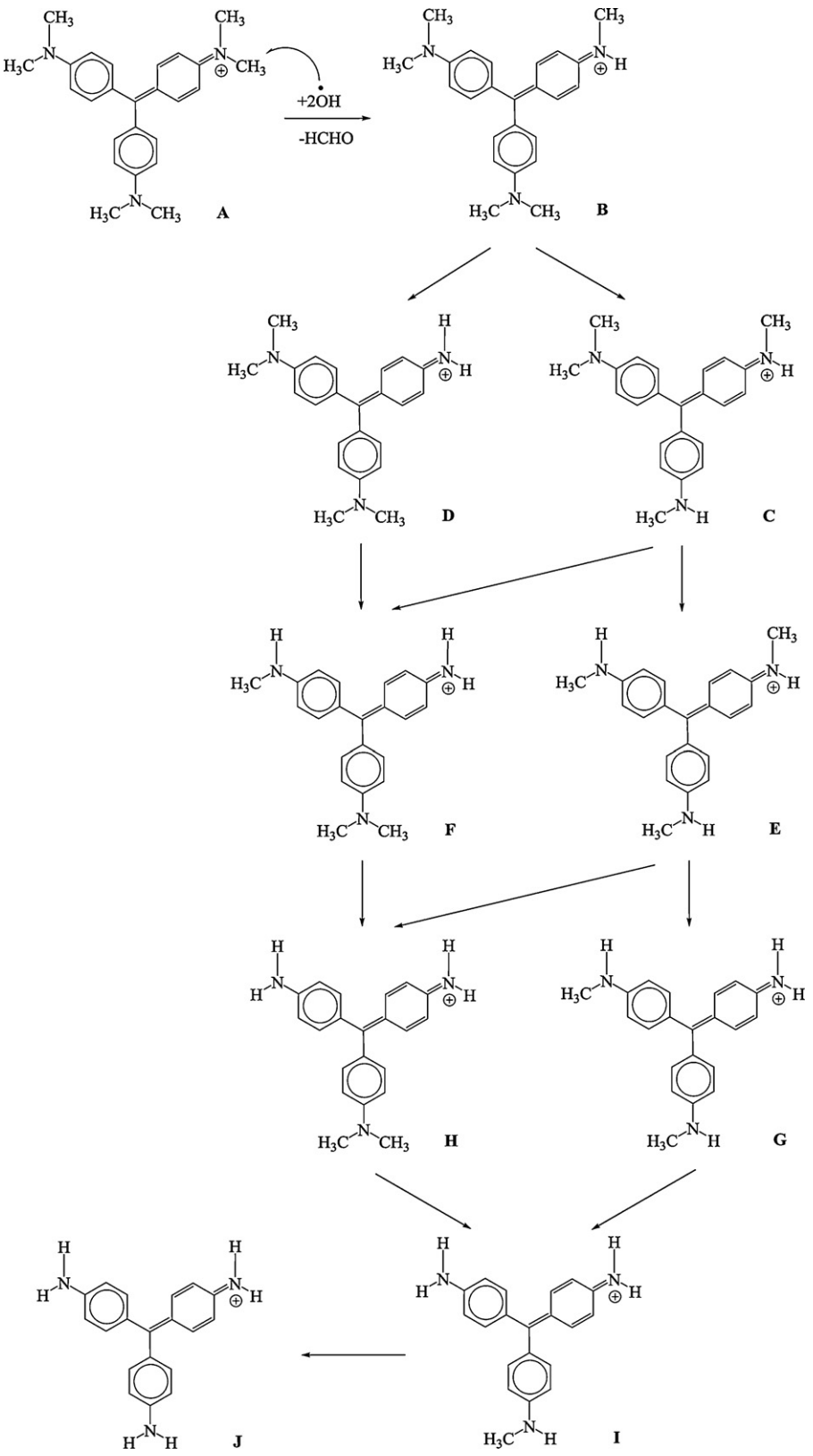

Fig. 11. Proposed *N*-de-methylation pathway of the CV dye under UV irradiation in the presence of Bi_2WO_6, according to the HPLC-ESI mass spectral results.

ious deprotonation pathways, which in turn are determined by the different adsorption modes of CV on the Bi_2WO_6 particles surface.

Base on the above experimental results, we tentatively proposed the photodegradation pathway depicted in Fig. 13. The dye molecule is adsorbed through the positively charged diethylamine functional group. The attraction of a hydrogen atom from the dimethylamine methyl group by one •OH radical, and the attack by another •OH radical on the dimethylamine results ultimately into *N*-de-methylation reaction. The mono-de-methylated dye intermediate, **B**, can also be adsorbed on the Bi_2WO_6 parti-

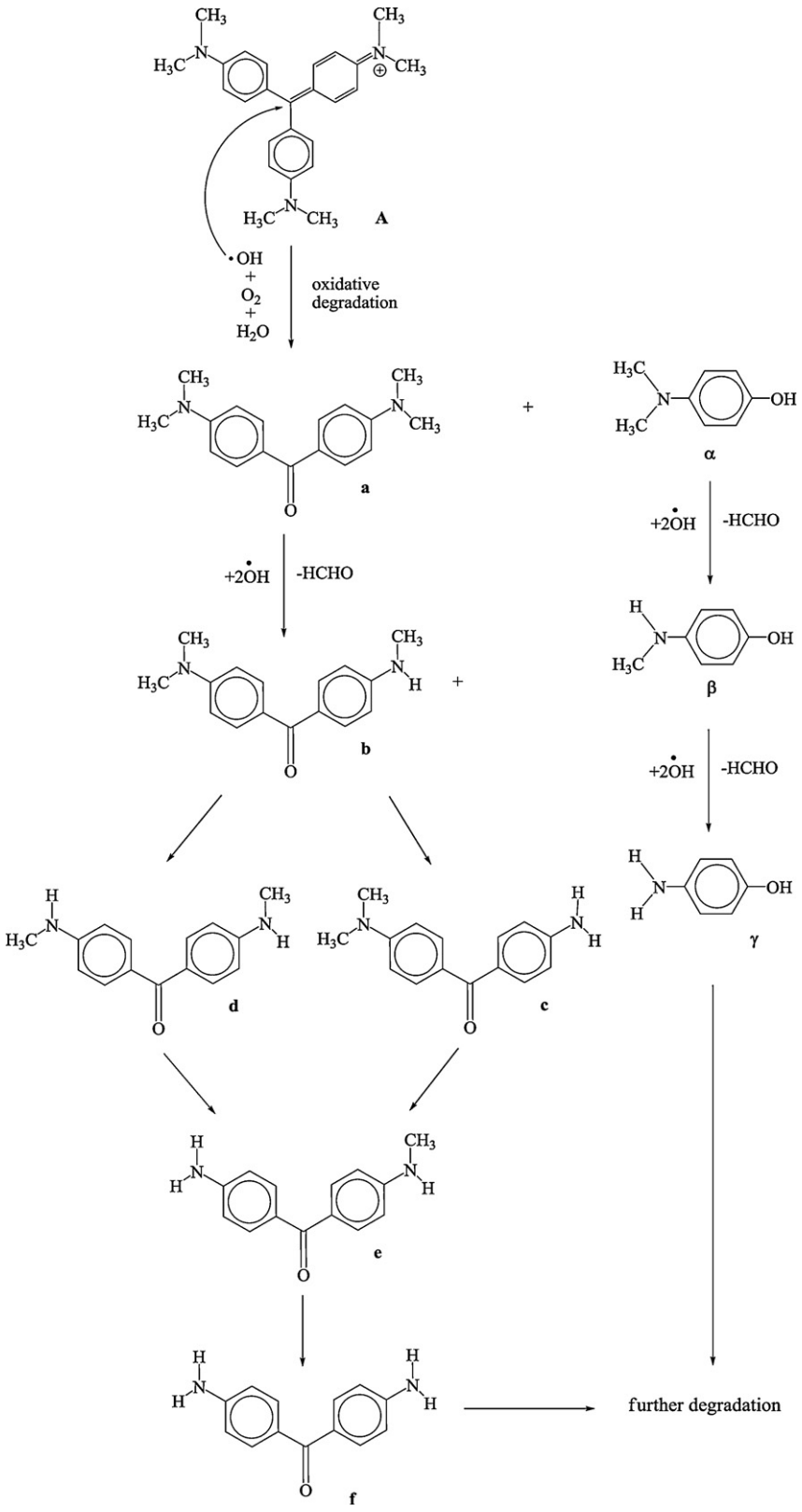

Fig. 12. Proposed pathways for the destruction of the CV dye conjugated structure under UV irradiation in the presence of Bi_2WO_6 according to the HPLC-ESI mass spectral results.

cle surface and is implicated similar events stepwise (•OH radicals attraction and attack, hydrolysis or deprotonation) to yield the bi-de-methylated dye derivatives, **C** and **D**. The *N*-de-methylation process as described above continues until the formation of the completely de-methylated dye, **J**.

Another degradation pathway as shown in Fig. 13, the CV dye molecule was adsorbed and through the conjugated structure of the CV chromophore, the attack of •OH radicals yield a carbon-centered radical, which subsequently was attacked by molecular oxygen leading ultimately to **a** and **α**. The **a** can also be adsorbed on the

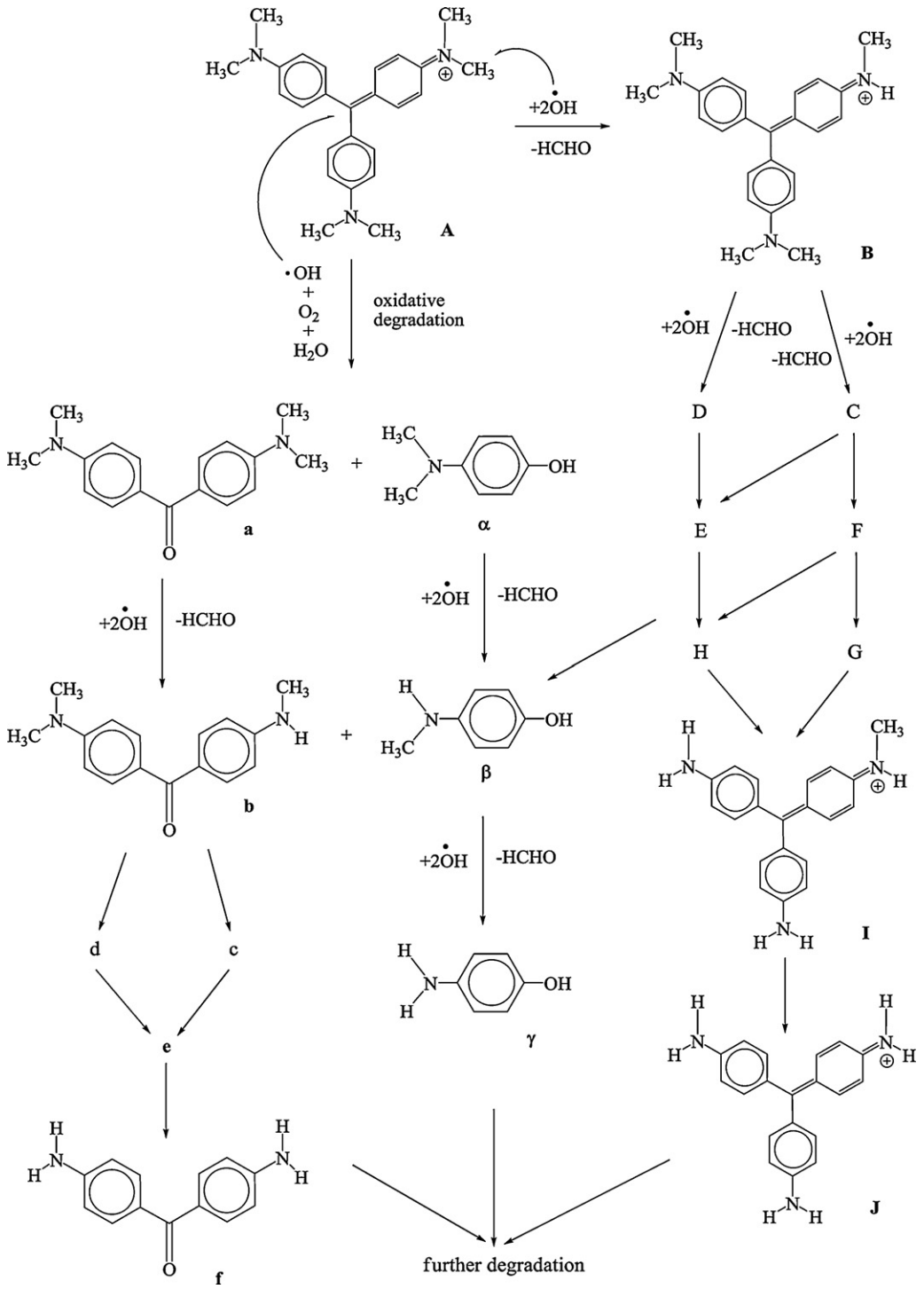

Fig. 13. A depict of overall photodegradation pathways for the CV dye under UV irradiation in the aqueous Bi_2WO_6 dispersions.

Bi_2WO_6 particle surface and be implicated in similar events (•OH radical attraction and attack, hydrolysis or deprotonation, and/or oxygen attack) to yield a di-*N*-de-methylated derivative, **b**, and the same process may occur in **α** to yield **β**. The *N*-de-methylation process as described above continues until formation of the completely *N*-de-methylated **f** and **γ**. The above *N*-de-methylation processes also produce a series of *N*-hydroxymethylated intermediates by the hydroxylation reaction on the *N*-methyl group. All the intermediates were further degraded to produce *N,N*-dimethylaminobenzene, *N*-methylaminobenzene, aminobenzene, acetamide, 2-propenoic acid, and acetic acid, which are subsequently mineralized and result in CO_3^{2-} and NO_3^- [48].

4. Conclusions

Square plate Bi_2WO_6 crystallite was prepared by the hydrothermal method in autoclave under alkaline condition, which served as a good candidate for the photocatalytic degradation of CV dye. The binding energy shift of the Bi suggested $Bi^{(+3-x)}$ formal oxidation state subjecting to the substoichiometric forms of Bi within the Bi_2O_2 layer. The *N*-de-methylation of the CV dye takes place in a

stepwise manner yielding a series of *N*-de-methylated intermediates until the formation of the completely *N*-de-methylated dye, and this was confirmed by the HPLC-PDA with gradual wavelength shifts of the maximum absorption band toward the blue region. Further evidences are obtained from the ESI/MS. The photodegradation mechanisms of UV/Bi_2WO_6 proposed in this study would hopefully shed some light for the future developments of technology applications for the decoloration of dyes.

Acknowledgement

This research was supported by the National Science Council of the Republic of China (NSC 99-2113-M-142-001-MY2).

References

[1] P.S. Berdonosov, D.O. Charkin, V.A. Dolgikh, S.Y. Stefanovich, R.I. Smith, P.J. Lightfoot, J. Solid State Chem. 177 (2004) 2632–2634.
[2] Y. Li, J. Liu, X. Hung, G. Li, Cryst. Growth Des. 7 (2007) 1350–1355.
[3] J. Ricote, L. Pardo, A. Castro, P. Millan, J. Solid State Chem. 160 (2001) 54–61.
[4] Z.G. Yi, Y.X. Li, Z.Y. Wen, S.R. Wang, J.T. Zeng, Q.R. Yin, Appl. Phys. Lett. 86 (2005) 192906–192909.
[5] M. Hamada, H. Tabata, T. Kawai, Thin Solid Films 306 (1997) 6–9.
[6] T. Zeng, H. Yan, H. Ning, J. Zeng, M.J. Reece, J. Am. Ceram. Soc. 92 (2009) 3108–3110.
[7] F. Amano, A. Yamakata, K. Nogami, M. Osawa, B. Ohtani, J. Am. Chem. Soc. 130 (2008) 17650–17651.
[8] J. Xu, W. Wang, M. Shang, S. Sun, J. Ren, L. Zhang, Appl. Catal. B: Environ. 93 (2010) 227–232.
[9] F. Amano, K. Nogami, M. Tanaka, B. Ohtani, Langmuir 26 (2010) 7174–7180.
[10] L.W. Zhang, Y.J. Wang, H.Y. Cheng, W.Q. Yao, Y.F. Zhu, Adv. Mater. 21 (2009) 1286–1290.
[11] G.Q. Zhang, N. Chang, D.Q. Han, A.Q. Zhou, X.H. Xu, Mater. Lett. 64 (2010) 2135–2137.
[12] X. Zhao, T. Xu, W. Yao, C. Zhang, Y. Zhu, Appl. Catal. B: Environ. 72 (2007) 92–97.
[13] M. Mączka, A.F. Fuentes, L. Kępiński, M.R. Diaz-Guillen, J. Hanuza, Mater. Chem. Phys. 120 (2010) 289–295.
[14] C. Zhang, Y.F. Zhu, Chem. Mater. 17 (2005) 3537–3545.
[15] H.B. Fu, L.W. Zhang, W.Q. Yao, Y.F. Zhu, Appl. Catal. B 66 (2006) 100–110.
[16] S.C. Zhang, C. Zhang, Y. Man, Y.F.J. Zhu, Solid State Chem. 179 (2006) 62–69.
[17] M. Shang, W.Z. Wang, S.M. Sun, L. Zhou, L. Zhang, J. Phys. Chem. C 112 (2008) 10407–10411.
[18] Y.Y. Li, J.P. Liu, X.T. Huang, G.Y. Li, Cryst. Growth Des. 7 (2007) 1350–1355.
[19] S. Yao, J. Wei, B. Huang, S. Feng, X. Zhang, X. Qin, P. Wang, Z. Wang, Q. Zhang, X. Jing, J. Zhan, J. Solid State Chem. 182 (2009) 236–239.
[20] J. Wu, F. Duan, Y. Zheng, Y. Xie, J. Phys. Chem. C 111 (2007) 12866–12871.
[21] L.S. Zhang, W.Z. Wang, L. Zhou, H.L. Xu, Small 3 (2007) 1618–1625.
[22] S.W. Liu, J.G.J. Yu, Solid State Chem. 181 (2008) 1048–1055.
[23] L. Zhang, W. Wang, L. Zhou, H. Xu, Small 3 (2007) 1618–1625.
[24] H. Takeda, T. Nishida, S. Okamura, T. Shiosaki, J. Eur. Ceram. Soc. 25 (2005) 2731–2734.
[25] G. Zhang, F. Lü, M. Li, J. Yang, X. Zhang, B. Huang, J. Phys. Chem. Solids 71 (2010) 579–582.
[26] S.O. Alfaro, A.M. Cruz, Appl. Catal. A 383 (2010) 128–133.
[27] Y. Li, J. Liu, X. Huang, G. Li, Cryst. Growth Des. 7 (2007) 1350–1355.
[28] G. Li, D. Zhang, J.C. Yu, M.K.H. Leung, Environ. Sci. Technol. 44 (2010) 4276–4281.
[29] F. Amano, A. Yamakata, K. Nogami, M. Osawa, B. Ohtani, J. Phys. Chem. C 113 (2009) 1536–1542.
[30] L. Wu, J. Bi, Z. Li, X. Wang, X. Fu, Catal. Today 131 (2008) 15–20.
[31] L.S. Zhang, W.Z. Wang, Z.G. Chen, L. Zhou, H.L. Xu, W. Zhu, J. Mater. Chem. 17 (2007) 2526–2532.
[32] (a) F. Amano, K. Nogami, R. Abe, B.J. Ohtani, Phys. Chem. C 112 (2008) 9320–9326;
(b) C.X. Xu, X. Wei, Z.H. Ren, Y. Wang, G. Xu, G. Shen, G.R. Han, Mater. Lett. 63 (2009) 2194–2197.
[33] T. Giesenberg, S. Hein, M. Binnewies, G. Kickelbick, Angew. Chem. Int. Ed. 43 (2004) 5697–5700.
[34] Y. Huang, Z. Ai, W. Ho, M. Chen, S. Lee, J. Phys. Chem. C 114 (2010) 6342–6349.
[35] Z. Cui, D. Zeng, T. Tang, J. Liu, C. Xie, Catal. Commun. 11 (2010) 1054–1057.
[36] J.H. Ryu, J. Alloys Compd. 441 (2007) 146–151.
[37] R. Harpeness, A. Gedanken, New J. Chem. 27 (2003) 1191–1193.
[38] C. Jovalekic, M. Pavlovic, P.L. Osmokrovic, Appl. Phys. Lett. 72 (1998) 1051–1054.
[39] L.Q. Jing, X.J. Sun, B.F. Xin, B.Q. Wang, W.M. Cai, H.G. Fu, J. Solid State Chem. 177 (2004) 3375–3382.
[40] S. Parra, S.E. Stanca, I. Guasaquillo, K.R. Thampi, Appl. Catal. B: Environ. 51 (2004) 107–116.
[41] J.C. Zhao, H. Hidaka, A. Takamura, E. Pelizzetti, N. Serpone, Langmuir 9 (1993) 1646–1650.
[42] X. Li, G. Liu, J. Zhao, New J. Chem. 23 (1999) 1193–1196.
[43] C.C. Chen, C.S. Lu, Environ. Sci. Technol. 41 (2007) 4389–4396.
[44] C.C. Chen, F.D. Mai, K.T. Chen, C.S. Lu, Dyes Pigments 75 (2007) 434–442.
[45] H.J. Fan, S.T. Huang, W.H. Chung, J.L. Jan, W.Y. Lin, C.C. Chen, J. Hazard. Mater. 171 (2009) 1032–1044.
[46] C.C. Chen, H.J. Fan, J.L. Jan, J. Phys. Chem. C 112 (2008) 11962–11972.
[47] C.C. Chen, C.S. Lu, J. Phys. Chem. C 111 (2007) 13922–13932.
[48] A.B. Prevot, C. Baiocchi, M.C. Brussino, E. Pramauro, P. Savarino, V. Augugliaro, G. Marci, L. Palmisano, Environ. Sci. Technol. 35 (2001) 971–976.